



Published in final edited form as:

Phys Med Biol. 2012 September 21; 57(18): 5749–5763. doi:10.1088/0031-9155/57/18/5749.

Non-contact respiration monitoring for in-vivo murine micro computed tomography: characterization and imaging applications

Laurel M Burk¹, Yueh Z Lee^{1,2}, J Matthew Wait¹, Jianping Lu¹, and Otto Z Zhou^{1,3,4}

Laurel M Burk: lmburk@physics.unc.edu

¹Department of Physics and Astronomy, University of North Carolina, Chapel Hill, NC 27599

²Department of Radiology, University of North Carolina, Chapel Hill, NC 27599

³Curriculum in Applied Sciences and Engineering, University of North Carolina, Chapel Hill, NC 27599

⁴Lineberger Comprehensive Cancer Center, University of North Carolina, Chapel Hill, NC 27599

Abstract

A cone beam micro-CT has previously been utilized along with a pressure-tracking respiration sensor to acquire prospectively gated images of both wild-type mice and various adult murine disease models. While the pressure applied to the abdomen of the subject by this sensor is small and is generally without physiological effect, certain disease models of interest, as well as very young animals, are prone to atelectasis with added pressure, or they generate too weak of a respiration signal with this method to achieve optimal prospective gating. In this work we present a new fiber-optic displacement sensor which monitors respiratory motion of a subject without requiring physical contact. The sensor outputs an analog signal which can be used for prospective respiration gating in micro-CT imaging. The device was characterized and compared against a pneumatic air chamber pressure sensor for the imaging of adult wild-type mice. The resulting images were found to be of similar quality with respect to physiological motion blur; the quality of the respiration signal trace obtained using the non-contact sensor was comparable to that of the pressure sensor and was superior for gating purposes due to its better signal-to-noise ratio. The non-contact sensor was then used to acquire in-vivo micro-CT images of a murine model for congenital diaphragmatic hernia and of 11-day-old mouse pups. In both cases, quality CT images were successfully acquired using this new respiration sensor. Despite the presence of beam hardening artifact arising from the presence of a fiber-optic cable in the imaging field, we believe this new technique for respiration monitoring and gating presents an opportunity for in-vivo imaging of disease models which were previously considered too delicate for established animal handling methods.

1. Background

The use of in-vivo micro-CT has been recently demonstrated for a variety of preclinical murine imaging applications (Ritman 2011). The high contrast between air and pulmonary tissue makes micro-CT particularly useful for studies of lung diseases such as lung carcinoma (Burk 2011a) and emphysema (Ford 2009); iodine-based blood pool agents provide superb contrast against soft tissue to permit studies of the heart (Mukundan 2006, Badea 2007, Drangova 2007, Detombe 2008, Burk 2011b) and vascular systems. However as a consequence of the animal's rapid respiration rate (~200 bpm conscious and ~120 bpm anesthetized), clinical breath-hold imaging techniques are not feasible. Some method of respiratory gating must be employed to reduce motion blur of the thorax when performing in vivo imaging of the heart and lungs.

Retrospective gating techniques (both intrinsic and extrinsic) have the benefit of easy implementation and fast scan times (Farncombe 2008, Bartling *et al* 2007, Ertel *et al* 2009, Ford *et al* 2007) but result in an increased radiation dose to the subject due to the resultant oversampling. Prospective gating circumvents this problem by synchronizing x-ray exposure with the physiological phase of interest. One possible method of prospective gating involves intubating subjects and directly manipulating airway pressure through a ventilator, controlling the amplitude and periodicity of the respiratory motion so that it matches x-ray exposure windows (Cavanaugh *et al* 2004, Walters *et al* 2004, Namati *et al* 2006). This protocol eliminates the wasted radiation dose of retrospective gating, but it requires advanced animal handling techniques to prevent damage to the trachea and vocal chords. At least one instance of repeated intubation is available in the literature (Brown *et al* 1999) without complications, but no information is available about limits to the frequency of the procedure or maximal number of procedures possible on a single animal. Additionally, the process of mechanical ventilation has been shown to induce lung injury in otherwise previously healthy specimens (Curley *et al* 2009, Hedlund and Johnson 2002, Vaneker *et al* 2009, Wolthus *et al* 2009). These risks mean that forced breathing and breath-hold gating methods are not ideal for longitudinal studies, particularly for sensitive disease models. Also, while external control of lung pressure and volume aids the imaging process, it can result in measures of tidal lung volumes and related values which are not accurate or physiologically relevant to the study.

A less invasive method of prospective gating permits free-breathing mice to be imaged by tracking respiratory chest motion of the animal with a pressure sensor or CCD camera and synchronizing x-ray pulses with a desired phase in the respiration cycle (Ford *et al* 2005, Cao *et al* 2009); this general approach is the focus of this paper. While the researcher does not have direct control of the physiological state of a free-breathing subject, it has been demonstrated that, in general, a healthy adult mouse under anesthesia and temperature control generally exhibits stable, quasi-periodic respiratory motion so that images of the thorax are blur-free (Ford *et al* 2005). The aforementioned technique has the drawback of increased scan times per CT image, but it keeps radiation dose to the subject low and does not require intubation (along with the associated risks). In order to achieve optimal results, one requires an x-ray source with good temporal resolution (100 ms or less to achieve blur-free respiration images according to Mai *et al* 2005) and reliable information about the position of the subject's lungs and abdomen at any given point of time.

In combination with a micro-CT scanner operating in step-and-shoot mode with short-duration, high flux x-ray pulses, a pneumatic air chamber sensor has been employed to track respiratory motion and gate prospectively to the desired breath phase. The technology has been successfully demonstrated for a variety of applications and disease models which require non-invasive imaging of adult mice (Cao 2010b, Lee 2011, Burk 2011a, Burk 2011b). To ensure a strong signal output, the pneumatic sensor typically requires some small amount of additional pressure to be applied around the abdomen, such as that resulting from an adhesive medical tape placed around the animal and sensor. This requires that the externally applied pressure be temporally uniform so that changes in the respiratory signal strength correspond directly with abdominal motion alone. Furthermore, while the applied pressure is generally small and does not affect a healthy adult animal or its breathing response in any obvious way, this is not necessarily the case for an animal with lung disease, structural deformity of the ribs, abdomen, or diaphragm. Neither is this guaranteed for an animal which has not reached physical maturity and whose small size and weight alone does not exert enough pressure on the air chamber sensor to give a strong signal without applying a greater external pressure to compensate. The consequences of exceeding an animal's tolerance for externally-applied pressure about the abdomen include temporary atelectasis, preventing an accurate measure of lung volume and other physiological information. At

worst, a delicate animal model might be permanently physically affected, or at least temporarily affected in a way that would obfuscate symptoms of the disease being tracked. An ideal method of abdominal position tracking would include no risk of physical impact to the subject and would involve no physical contact with the subject. Such a tool would allow non-invasive quantitative assessment of lung function without perturbation by the compressive band required with a pressure-based respiration sensor.

To avoid this problem, one might make do with non-gated imaging (and the inevitable motion blur in the abdomen) or employ an alternative, contactless method of respiration monitoring. Novel contactless respiration tracking has been demonstrated for the human clinical setting including methods such as laser monitoring of the chest wall location (Kondo *et al* 1997) and electromagnetic sensing (Scalise *et al* 2011). In small animal imaging, intrinsic gating (Bartling *et al.* 2008) does not require physical contact with the subject, although the gating is retrospective in nature and requires an additional radiation dose when compared with prospective methods. In our previous work with in vivo murine micro-CT, we have refined a prospective technique for respiration gating using the output of a pneumatic air chamber sensor, and we would prefer to use a displacement-measurement sensor which does not require physical contact with the subject but which generates a familiar output trace matching that from the pneumatic sensor. With this in mind, a fiber-optic laser displacement sensor setup was developed to incorporate a commercially-available fiber optic sensor (Philtex Inc., Annapolis MD) into the BioVet physiological monitoring system (m2m Imaging Corp, Cleveland OH) that tracks the signal from the respiration pressure sensor. A voltage-splitting circuit and high-pass filter were added to best replicate the familiar respiration wave shape free of added noise or a DC offset, which allowed the use of signal amplification through BioVet.

This new non-contact sensor and our conventional pressure sensor were both tested for the gated imaging of wild type mice; the quality of the respiration traces and the resulting images were compared. Finally, we employed this sensor to obtain prospectively-gated in-vivo images of models which were previously unattainable using established techniques: a congenital diaphragmatic hernia model in which bowel contents have herniated into the thoracic cavity, and 11-day-old mouse pups.

2. Materials/Methods

2.1 Hardware

The contactless sensor developed for non-invasive respiration monitoring is based on a fiber optic displacement sensor with analog amplified output (Philtex RC60-C8T35 Fiber Optic Analog Amplifier). It consists of a small rectangular sensor tip from which the laser signal exits perpendicularly, reflects from a nearby surface (either dull or reflective) and is picked up again by the sensor tip. The sensor is connected to the electronics housing via long, thin fiber optic bundles which carry the optical signal out to and back from the tip without significant loss. The ratio of signal strength between the output and measured reflected light is used as a surrogate for the distance between the sensor tip and the reflective surface, allowing sensitive measurements of small displacements to be converted into an output direct current voltage of 0–5V. After the addition of a voltage-splitter and high-pass filter to remove a direct current offset, this signal is input into our current BioVet monitoring system so that the signal enhancement and gating triggering features of that hard- and software can be utilized as a comparison with BioVet's established pneumatic pressure sensor.

An animal bed composed of acrylonitrile butadiene styrene (ABS) plastic (Figure 1) was designed to allow the subject to be positioned prone with the noncontact sensor's tip stabilized next to the ribcage at a gap distance of a few millimeters from skin to signal-exit

surface. This was achieved by modifying a bed which interfaces with the pneumatic air chamber sensor, adding a rectangular slot in the support wings into which the sensor was inserted with emission-tip oriented facing the chest. The emission tip must be perpendicular to the measured surface for proper results. A reflective surface was not required for use of this displacement sensor; either bare skin or fur allowed enough signal reflection for the sensor to receive a strong usable signal for respiration gating. For the purposes of all in-vivo studies mentioned in this paper, no shaving or other manipulation of the subject's fur was performed. Subtle abdominal movements of 1 mm or less are easily detected using the fiber optic displacement sensor, in accordance with the specifications provided by Philtec, Inc.

CT images were acquired using a custom-built field emission x-ray cone beam micro-CT (Cao 2010b; Lee 2011) with a 100 μm effective focal spot size, 1.3 geometry magnification, and 20 degree cone beam angle. The scanner was operated in a step-and-shoot mode with 400 projections acquired over a total 200 degrees of gantry rotation. All images were acquired with 50kVp x-rays and an additional 0.5mm Al filter between the source and object, with the cathode current and exposure time adjusted to suit the desired application and gating requirements. Physiological information from the animal was gathered and monitored using BioVet software, with respiration signal derived from either the pressure sensor (in comparison testing) or non-contact sensor (for comparison testing and imaging studies). In the former setup, the pneumatic sensor was placed beneath the animal's abdomen while in prone position. In the latter, the non-contact displacement sensor was placed next to the animal's ribcage (a few millimeters gap distance) in a slot built into the wings of the animal bed. In both cases, the signal was read into the BioVet program and appropriate threshold levels were selected for gating. When the preset gating threshold was reached and it fell within the readout phase of the 1 Hz fixed-frame rate detector, then the x-ray source was triggered and a single projection image was acquired. After gantry rotation to the next position, the procedure was repeated until the full number of projection images had been acquired (all in the same phase of the respiratory cycle), with a typical imaging time of 8–15 minutes depending upon the animal's physiology. The radiation dose for each scan was 12.5 cGy. After acquisition, images were preprocessed with a custom MATLAB program to remove dark lines and pixels and then were reconstructed with a Feldkamp algorithm using the commercial reconstruction software COBRA (Exxim Computing Corporation, Pleasanton CA). The images were reconstructed at a voxel size of 77 microns.

2.2 In vivo studies

All animal imaging studies were performed in accordance with a protocol approved by the Institutional Animal Care and Use Committee at the University of North Carolina at Chapel Hill.

2.2.1 Wild-type subjects—Respiration-gated in vivo cone beam CT was performed on four wild-type (C57BL/6N) male mice with masses ranging from 25 to 30 grams, using the previously described imaging parameters, 30 ms x-ray pulses and a 1.67 mA tube current. Subjects were initially anesthetized using a mix of oxygen and 2.5% isoflurane and were then maintained at a mix of 1.0–1.5% isoflurane and were free-breathing for the duration. Anesthesia dosage was adjusted to maintain stable respiration, with rates of 93 ± 8 bpm for both pressure and noncontact sensors for all subjects. The total imaging time was approximately 15 minutes and subjects were under anesthesia for a total of approximately 25 minutes. Two sets of images were acquired, with triggering first by the pneumatic pillow sensor and then by the contactless sensor. Each animal was imaged first during the peak inhalation phase, and then three of the four animals were then re-imaged at the full exhalation phase so that utility of the technique could be shown for both major phases of respiration. This versatility of respiration phase is necessary for volumetric lung imaging.

Both pieces of hardware were kept in the imaging field of view during all scans to control for any resulting imaging artefacts. Each sensor registered the same respiration rate during imaging; a more detailed comparison in the case of wild-type adults is the subject of section 3.1; this matching of breath shape and rate was seen for all animals and models studied in this work.

The signals from the two sensors were analysed and compared in terms of both signal strength and shape in order to justify using their outputs interchangeably for physiological gating. To quantitatively assess the shapes of breaths measured by each sensor, we noted the timepoint corresponding to the maximum signal output (point of maximum inhalation) and compared the results between the non-contact and pneumatic sensors for all subjects. Additionally, we measured the signal outputs of the sensors over an average breath (averaged over 400 breaths) for each of the four subjects, sampling every 2 ms, and then plotted these results as comparison curves to assess the subtle differences in breath signal shape resulting from the distinct mechanisms underlying the function of the two respiration sensors (pressure versus position).

Both qualitative and quantitative comparisons between the two sets of micro-CT images were made to assess overall image quality. As a surrogate measurement of physiological motion blur present in the gated images, a measurement of average diaphragm slope was taken for each set. This was achieved by identifying four lines across the transition from lower lung to diaphragm (two in the left lung and two in the right lung) and calculating the slope in HU/pixel of these paths as they crossed the boundary. These four values were averaged together to give a single diaphragm slope for each CT image; in this way, motion blur effects from each of the two gating protocols could be compared quantitatively.

After establishing the characteristics of the noncontact sensor and its derived respiration signal, we demonstrated its application with specific in-vivo imaging studies, including a model for congenital diaphragmatic hernia in adult mice and a model for cystic fibrosis in 11-day-old mouse pups.

2.2.2 Congenital diaphragmatic hernia model—The first candidate for imaging with non-contact respiration gating was a murine model for congenital diaphragmatic hernia developed by suppression of the *Slit3* gene (Yuan 2003, Clugston 2006). The disease is characterized by deformation of the diaphragm in infants which allows the lower organs to breach the diaphragm wall and displace the lungs, causing pulmonary hypoplasia and pulmonary hypertension. To study the progression of this disease longitudinally, respiration-gated micro-CT was considered as a diagnostic tool; however, the characteristic diaphragmatic weakness of this disease made the model a poor choice for any imaging which would require pressure to be applied at the abdomen. Even if images could successfully be acquired, it would be uncertain whether the applied pressure from a pneumatic sensor would exacerbate the physical characteristics of the disease and lead to misrepresentative results. Fortunately, development of a non-contact displacement sensor allowed in-vivo micro-CT to be performed without any physical manipulation of the study subjects. Two adult male and two adult female animals of a 129x1/SvJ/C57BL/6 mix with masses between 20 and 25 grams were imaged using the protocol discussed in section 2.1. One each of each sex were *Slit3* $-/-$ and had diaphragmatic hernias; the other two were *Slit3* $+/+$ and displayed the normal phenotype. Immediately prior to imaging, an iodinated contrast agent (Fenestra VC, ART Advanced Research Technologies Inc, Montreal Canada) was applied intravenously through the tail vein in a bolus at the recommended dosage of 0.1mL/mg body weight. Subjects were initially anesthetized using a mix of oxygen and 2.5% isoflurane and were then maintained at a mix of 1.0–1.5% isoflurane and were free-breathing for the duration. Anesthesia dosage was adjusted to maintain stable respiration,

with rates of 98 ± 15 bpm for all subjects. The total imaging time was approximately 15 minutes and subjects were under anesthesia for a total of approximately 25 minutes. In this application, only the contactless respiration sensor was used for triggering the gated images. 400 step-and-shoot projections were acquired over 200 degrees gantry rotation in 30 ms x-ray pulses gated to the maximum inhalation phase of the respiration cycle with a tube current of 1.67 mA. The 50 kVp x-rays were filtered with 0.5 mm of aluminium after exiting the 0.2 mm beryllium window.

2.2.3 11-day old mouse pups—Another consequence of the development of a non-contact respiration sensor was the capability to image mouse pups in the one to two week age range. Amongst the challenges discovered in our previous effort to image mice at this age were their small size (ten grams or less) and the correspondingly weak respiration signal transmitted through the pressure sensor when placed beneath them. In past attempts to utilize the pressure sensor for respiratory-gated imaging, we found that by adding pressure with the elastic medical tape about the abdomen, animal instability was increased. The lightly-anesthetized pups would be more prone to motion, with both gasps and intermittent kicks which in turn resulted in significant artifacts. Moreover, the likelihood of atelectasis of some or most of the left lung was much greater in the imaging of these pups than their adult counterparts.

Non-invasive imaging of mouse pups is desirable for disease models in which interesting physiological changes occur within less than a month of age. Such is the case for the Scnn1b-Tg murine model of cystic fibrosis (Mall 2004, Mall 2008), in which tracheal mucus obstruction leads to neonatal mortality in some subjects while their littermates survive to maturity (Livraghi 2009). This model has been imaged at ages as early as a few days to six weeks using ungated, high-speed volumetric computed tomography (Wielputz 2011), but the resulting spatial resolution is inferior to that of physiologically-gated imaging. As a demonstration of our capability for imaging young subjects with non-contact CT techniques, we performed respiration-gated micro-CT on four 11-day-old wild-type animals (C57BL/6N), with an average mass of 4.4 ± 0.3 g. CTs were acquired both with and without prospective respiration gating. Subjects were initially anesthetized using a mix of oxygen and 2.5% isoflurane and were then maintained at a mix of 1.0–1.5% isoflurane and were free-breathing for the duration. Dosage was adjusted to maintain stable respiration, with rates of 57 ± 10 for both pressure and noncontact sensors for all subjects. The total imaging time was approximately 15 minutes and subjects were under anesthesia for a total of approximately 25 minutes. The protocol for these images was to acquire 400 step-and-shoot projections over 200 degrees gantry rotation. 35 ms x-ray pulses at 1.5 mA tube current were gated to the maximum inhalation phase of the respiration cycle using the contactless sensor for triggering. The 50 kVp x-rays were filtered with 0.5 mm of aluminum after exiting the 0.2 mm beryllium window.

3. Results

3.1 Comparison of non-contact sensor to pneumatic pressure sensor

For each of the four adult wild-type mice, simultaneous measurement of respiration data was acquired from both the pressure and noncontact sensors; an image of the BioVet software interface displaying both respiration traces simultaneously is shown in figure 4. With the chosen placement of the noncontact sensor tip in relation to the subject's ribcage, signal traces closely match in both period and shape, and in particular the peak of the signal shape from both sensors matches temporally. As these signals are used to determine the timepoint at which x-rays are fired, matching signals result in identical timing of the x-ray pulses. Moreover, the enhanced sensitivity of the laser displacement sensor over the pressure sensor results in reduced need for the signal amplification through the BioVet hardware. This

results in a greater signal to noise ratio and a cleaner respiration signal for gating, reducing the likelihood of pulse mistiming due to electrical noise.

Images obtained with both the noncontact sensor (figure 5a) and the pneumatic pressure sensor (figure 5b) are not obscured by compression-induced atelectasis. Just as the respiration signal traces from the two sensors were nearly identical in shape, the image quality of both sets of images is comparable. The extent of motion blur in the diaphragm is consistent between gating methods, as is the fine structure detail in the lungs visible in transverse slices. A noticeable streak artifact arises in both sets of images due to the presence of the highly-attenuating fiber-optic cable which was kept in place even during the pressure-sensor imaging for consistency of the comparison experiment. Even with the artifact present, many qualitative observations can be made of the subject's physiology, though the results of quantitative density measurements and some volume measurements obtained through automatic segmentation programs may be distorted. Nonetheless, the diagnostic value of these images is still far greater than that of micro-CT images obscured by pressure-induced atelectasis.

Respiratory motion blur, as quantified by the slope of the line plot across the lung/diaphragm boundary, does not vary significantly between images obtained with the two different respiration sensors (Table 1). The average slopes resulting from the non-contact and pressure protocols were 141 HU/pixel and 140 HU/pixel, respectively. The variation of slopes for subjects within a given gating protocol is much greater than the variation between protocols, which implies that image quality with respect to motion blur is essentially the same using either respiration sensor. Other factors not controlled for in this comparison, such as animal handling and the stability and health of the subject, can have an even greater impact on image quality. This is because proper respiration gating through any method relies on consistent breath depth even though true periodicity is not required; if lung volume varies appreciably over the total scan time, motion artifacts will arise.

3.2 Imaging Applications

3.2.1 Congenital diaphragmatic hernia model—Images were successfully obtained for four age-matched male animals, two wild-type mice and two animals with congenital diaphragmatic hernias. With the presence of blood pool iodinated contrast agent, CTs of the wild-type animals display healthy heart and lungs (figure 7a) and vasculature of the liver (figure 7b) with expected physiology. The presence of the fiber optic cable in the most anterior slices resulted in dark-streak beam hardening (figure 7a) which nonetheless did not obscure qualitative results. No such streak artifact is visible in the mid-liver slice (figure 7b), as the sensor position did not extend that far in the posterior direction.

A striking difference was observed in the CT images of the diaphragmatic hernia model animals in both axial slices shown in figure 7. A large volume of the right lung has been displaced by the liver and other organs crossing the diaphragm, and the presence of iodine in the blood pool visualizes that the heart is compressed and distorted in shape (left). In the lower axial slice where one would expect only the base of the lungs and the liver, lower organs are visible. Because the respiration monitoring apparatus did not involve applied pressure, or any direct contact with the subject, these results are unquestionably the result of disease progression and not influenced by animal handling during image acquisition.

3.2.2 11-day old mouse pups—Micro-CT images of 11-day-old mouse pups imaged using prospective respiration gating from the laser-displacement non-contact sensor are shown in figures 9b and 9d. Transverse slices of the lungs show details of fine pulmonary structures which are more clearly visible in gated imaging (9b) than without gating (9a), and coronal slices (9d) demonstrate a sharp contrast across the diaphragm which is an indication

of low respiratory motion blur, compared with the non-gated comparison CT image (figure 9c). In addition to the overall image quality, no atelectasis was observed in any of the pups imaged using the non-contact sensor. In contrast, the earlier CT images of mouse pups acquired using the pneumatic pressure sensor and Coban tape compression (figure 8) demonstrate severe atelectasis and as a result provide no useful data on the structure or function of the left lung.

4. Discussion

We have presented a new method of respiration monitoring and gating which broadens the possible applications for in vivo prospectively gated cone beam micro-CT imaging. The quality of the respiration signal from the noncontact displacement sensor is equal to or superior to that from a pneumatic air chamber pressure sensor and transducer, and the signal shapes from both detectors are so similar that no modification of the method of physiological triggering for imaging is necessary. In a comparison of in vivo micro-CT of wild-type adult mice using both respiration sensors, the image quality was comparable except for the presence of the x-ray-opaque fiber optic cable in the field of view and its resulting artefacts. For disease models prone to atelectasis when subject to mild abdominal compression, the noncontact displacement sensor allowed diagnostically useful in vivo CT imaging that would not be achievable using formerly established methods.

A major limitation to wide-spread utilization of this new fiber optic displacement sensor is the cable itself, which with our current micro-CT beam energy, filtration and standard reconstruction technique causes moderate to severe beam hardening artifacts in the most anterior slices. This is especially problematic as the lung and heart regions are those which most require prospective respiration gating for successful in-vivo imaging. Without correcting or preventing this artifact, the image quality obtained using the new noncontact sensor in the majority of imaging applications is still inferior to our previously established gating method using the pressure respiration sensor; however, for the special applications discussed in this paper this reduction in image quality is acceptable when physiologically-gated imaging would otherwise not be achievable. One possibility for future work involves placing the sensor closer at the subject's lower abdomen, away from the region of interest. However, the respiration motion of lower regions is substantially different from the chest in both magnitude and shape, so that the derived signal will not match the familiar respiration trace of the pneumatic sensor and our established gating protocol will need to be modified. Alternatively, the x-ray opaque fiber optic cable could be replaced with a more radiolucent alternative material. Nonetheless, it should be stressed that reconstruction technique employed for these studies was a Feldkamp algorithm with no further corrections for beam hardening and streaking artifacts. Much work has been done by others to tackle this class of reconstruction artifact, and such advanced reconstruction techniques could be employed to complement the non-contact protocol we have outlined. Presented without any additional correction, the images displayed in this paper are a worst-case-scenario of image quality, and we believe that the effects of beam hardening on image quality could be greatly reduced while maintaining the demonstrated animal-handling benefits of a contactless respiration sensor.

5. Conclusions

We have demonstrated that a non-contact respiration sensor based on fiber optics broadens the potential application for in vivo micro-CT of mice, extending this tool for use with mouse pups and adult murine models for diaphragmatic hernia and other similarly restrictive abdominal deformations. For the imaging of healthy adult mice and models which can withstand light pressure on the abdomen, traditional methods of respiration gating are still

preferable due to artefacts arising from the fiber optic cable, though these artefacts could be prevented or removed using other reconstruction techniques. While the sensor was developed for small animal x-ray imaging, it could be equally applied to any physiologically-gated imaging modality without loss of functionality. In this work we successfully employed the non-contact sensor along with a CNT field emission x-ray micro-CT to perform prospectively gated imaging.

Acknowledgments

This study was supported by grant U54CA119343 from the National Cancer Institute (Bethesda, MD) and C-CCNE ARRA Supplemental Award Number 3-U54-CA119343-05S2.

The authors would like to acknowledge Dr. Alessandra Livraghi-Butrico of the University of North Carolina CF Research Center, Dr. Sean McLean of the UNC Department of Pediatric Surgery, and Dr. Arjun Deb of the UNC Department of Cell and Molecular Physiology for providing the animal disease models discussed in this paper as well as the control wild-type mice.

References

- Badea CT, Hedlund LW, Boslego Mackel JF, Mao L, Rockman HA, Johnson GA. Cardiac microcomputed tomography for morphological and functional phenotyping of muscle LIM protein null mice. *Molecular Imaging: Official Journal of the Society for Molecular Imaging*. 2007; 6:261–8.
- Bartling SH, Stiller W, Grasruck M, Schmidt B, Peschke P, Semmler W, Kiessling F. Retrospective motion gating in small animal CT of mice and rats. *Investigative Radiology*. 2007; 42(10):704–714. [PubMed: 17984768]
- Bartling SH, Dinkel J, Stiller W, Grasruck M, Madisch I, Kauczor HU, Semmler W, Gupta R, Kiessling F. Intrinsic respiratory gating in small-animal CT. *European Radiology*. 2008; 18:1375–85. [PubMed: 18431578]
- Brown RH, Walters DM, Greenberg RS, Mitzner W. A method of endotracheal intubation and pulmonary functional assessment for repeated studies in mice. *J Appl Physiol*. 1999; 87(6):2362–5. [PubMed: 10601190]
- Burk, LM.; Lee, YZ.; Heathcote, S.; Wang, K.; Kim, WY.; Lu, JP.; Zhou, O. Medical Imaging 2011: Biomedical Applications in Molecular, Structural, and Functional Imaging. Lake Buena Vista; Florida, USA: 2011a. Carbon nanotube based respiratory gated micro-CT imaging of a murine model of lung tumors with optical imaging correlation; p. 79651L1-6.
- Burk, LM.; Wang, K.; Kang, E.; Rojas, M.; Willis, M.; Lee, YZ.; Lu, JP.; Zhou, O. Medical Imaging 2011: Biomedical Applications in Molecular, Structural, and Functional Imaging. Lake Buena Vista; Florida, USA: 2011b. Imaging of myocardial infarction using carbon nanotube micro-computed tomography and delayed contrast enhancement; p. 79651N1-6.
- Cao G, Lee YZ, Peng R, Liu Z, Rajaram R, Calderon-Colon X, An L, Wang P, Phan T, Sultana S, Lalush DS, Lu JP, Zhou O. A dynamic micro-CT scanner based on a carbon nanotube field emission x-ray source. *Phys Med Biol*. 2010a; 54:2323–40. [PubMed: 19321922]
- Cao G, Burk LM, Lee YZ, Calderon-Colon X, Shabana S, Lu JP, Zhou O. Prospective-gated cardiac micro-CT imaging of free-breathing mice using carbon nanotube field emission x-ray. *Medical Physics*. 2010b; 37:5306–5312. [PubMed: 21089765]
- Cavanaugh D, Johnson E, Price RE, Kurie J, Travis EL, Cody DD. In vivo respiratory-gated micro-CT imaging in small-animal oncology models. *Molecular Imaging*. 2004; 3(1):55–62. [PubMed: 15142412]
- Clugston RD, Klattig J, Englert C, Clagett-Dame M, Martinovic J, Benachi A, Greer JJ. Teratogen-induced, dietary and genetic models of congenital diaphragmatic hernia share a common mechanism of pathogenesis. *The American Journal of Pathology*. 2006; 169:1541–9. [PubMed: 17071579]
- Coleman AJ, Sinclair M. A beam-hardening correction using dual-energy computed tomography. *Phys Med Biol*. 1985; 30:1251–56. [PubMed: 4080822]

- Curley GF, Kevin LG, Laffey JG. Mechanical Ventilation: Taking Its Toll on the Lung. *Anesthesiology*. 2009; 111(4):701–3. [PubMed: 19707117]
- Detombe SA, Ford NL, Xiang F, Lu X, Feng Q, Drangova M. Longitudinal follow-up of cardiac structure and functional changes in an infarct mouse model using retrospectively gated micro-computed tomography. *Investigative Radiology*. 2008; 43:520–529. [PubMed: 18580335]
- Drangova M, Ford NL, Detombe SA, Wheatley AR, Holdsworth DW. Fast retrospectively gated quantitative four-dimensional (4D) cardiac micro computed tomography imaging of free-breathing mice. *Investigative radiology*. 2007; 42:85–94. [PubMed: 17220726]
- Ertel D, Kyriakou Y, Lapp RM, Kalender WA. Respiratory phase-correlated micro-CT imaging of free-breathing rodents. *Physics in Medicine and Biology*. 2009; 54(12):3837–3846. [PubMed: 19491456]
- Farncombe TH. Software-based respiratory gating for small animal conebeam CT. *Medical Physics*. 2008; 35(5):1785–1792. [PubMed: 18561653]
- Ford NL, Foster PJ, Nikolov HN, CJ, Norley D, Thornton MM, Drangova M, Holdsworth DW. Prospective respiratory-gated micro-CT of free breathing rodents. *Medical physics*. 2005; 32(9):2888–98. [PubMed: 16266103]
- Ford NL, Martin EL, Lewis JF, RA, Veldhuizen W, Drangova M, Holdsworth DW. In vivo characterization of lung morphology and function in anesthetized free-breathing mice using microcomputed tomography. *Journal of applied physiology*. 2007; 102(5):2046–55. [PubMed: 17255374]
- Hedlund LW, Johnson GA. Mechanical ventilation for imaging the small animal lung. *ILAR Journal/ National Research Council, Institute of Laboratory Animal Resources*. 2002; 43(3):159–174.
- Herman GT, Trivedi SS. A comparative study of two postreconstruction beam hardening correction methods. *IEEE Trans Med Imag*. 2010; 2:128–35.
- Hsieh J, Molthen RC, Johnson RH, Dawson CA. An iterative approach to the beam hardening correction in cone beam CT. *Med Phys*. 2000; 27:23–9. [PubMed: 10659734]
- Kondo T, Uhlig T, Pemberton P, Sly PD. Laser monitoring of chest wall displacement. *Eur Respir J*. 1997; 10:18659.
- Kyriakou Y, Meyer E, Prell D, Kachelrieß M. Empirical beam hardening correction (EBHC) for CT. *Med Phys*. 2010; 37:5179–87. [PubMed: 21089751]
- Lee YZ, Burk LM, Wang K, Cao G, Volmer J, Lu JP, Zhou O. Prospective respiratory gated carbon nanotube micro computed tomography. *Acad Radiol*. 2011; 18:588–93. [PubMed: 21377908]
- Livraghi A, Grubb BR, Hudson EJ, Wilkinson KJ, Sheehan JK, Mall MA, O’Neal WK, Boucher RC, Randell SH. Airway and Lung Pathology Due to Mucosal Surface Dehydration in β -Epithelial Na⁺ Channel-Overexpressing Mice: Role of TNF- α and IL-4R α Signaling, Influence of Neonatal Development, and Limited Efficacy of Glucocorticoid Treatment. *Journal of Immunology*. 2009; 182:4357–67.
- Mai W, Badea CT, Wheeler CT, Hedlund LW, Johnson GA. Effects of breathing and cardiac motion on spatial resolution in the microscopic imaging of rodents. *Magnetic resonance in medicine: official journal of the Society of Magnetic Resonance in Medicine/Society of Magnetic Resonance in Medicine*. 2005; 53:858–65. [PubMed: 15799053]
- Mall M, Grubb BR, Harkema JR, O’Neal WK, Boucher RC. Increased airway epithelial Na⁺ absorption produces cystic fibrosis-like lung disease in mice. *Nat Med*. 2004; 10:487–493. [PubMed: 15077107]
- Mall MA, et al. Development of chronic bronchitis and emphysema in beta-epithelial Na⁺ channel-overexpressing mice. *Am J Respir Crit Care Med*. 2008; 177:730–742. [PubMed: 18079494]
- Mukundan S Jr, Ghaghada KB, Badea CT, Kao CY, Hedlund LW, Provenzale JM, Johnson GA, Chen E, Bellamkonda RV, Annapragada A. A liposomal nanoscale contrast agent for preclinical CT in mice. *AJR American Journal of Roentgenology*. 2006; 186:300–7. [PubMed: 16423931]
- Namati E, Chon D, Thiesse J, Hoffman EA, de Ryk J, Ross A, McLennan G. In vivo micro-CT lung imaging via a computer-controlled intermittent iso-pressure breath hold (IIBH) technique. *Physics in medicine and biology*. 2006; 51(23):6061–75. [PubMed: 17110770]
- Ritman EL. Current status of developments and applications of micro-CT. *Annu Rev Biomed Eng*. 2011; 13:531–52. [PubMed: 21756145]

- Scalise, L.; De Leo, A.; Mariani Primiani, V.; Russo, P.; Shahu, D.; Cerri, G. Non contact monitoring of the respiration activity by electromagnetic sensing. Proceedings of IEEE International Symposium on Medical Measurements and Applications; Bari, Italy. 2011. p. 418-22.
- Vaneker M, et al. Mechanical ventilation induces a Toll/interleukin-1 receptor domain-containing adapter-inducing interferon beta-dependent inflammatory response in healthy mice. *Anesthesiology*. 2009; 111(4):836–43. [PubMed: 19741489]
- Walters EB, Panda K, Bankson JA, Brown E, Cody DD. Improved Method of in vivo respiratory-gated micro-CT imaging. *Physics in Medicine and Biology*. 2004; 49:4163–4172. [PubMed: 15470930]
- Wielputz MO, Eichinger M, Zhou Z, Leotta K, Hirtz S, Bartling SH, Semmler W, Kauczor HU, Puderbach M, Mall MA. In vivo monitoring of cystic fibrosis-like lung disease in mice by volumetric computed tomography. *Eur Respir J*. 2011; 38:1060–70. [PubMed: 21478215]
- Wolthuis EK, Vlaar APJ, Choi G, Roelofs JJTH, Juffermans NP, Schultz MJ. Mechanical ventilation using non-injurious ventilation settings causes lung injury in the absence of pre-existing lung injury in healthy mice. *Critical Care*. 2009; 13(1):R1. [PubMed: 19152704]
- Yuan W, Rao Y, Babiuk RP, Greer JJ, Wu JY, Ornitz DM. A genetic model for a central (septum transversum) congenital diaphragmatic hernia in mice lacking Slit3. *PNAS*. 2003; 100(9):5217–5222. [PubMed: 12702769]

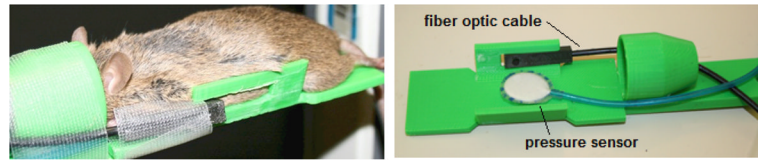


Figure 1.

The plastic mouse bed allows the animal to lie prone with its head inside the nose cone for gaseous anesthesia delivery, and the non-contact displacement sensor is positioned a few millimeters away from the animal's ribs. The design allows simultaneous testing of the pressure and non-contact sensors with murine subjects.

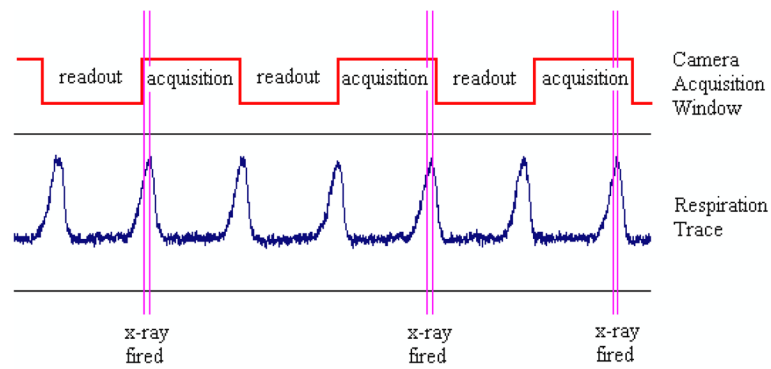


Figure 2.

A schematic of the timing structure employed in prospective gating is shown above. X-rays are to be fired only during the maximum inhalation phase of respiration, but this must also fall within the acquisition window of the fixed-frame rate flat panel detector. When these two conditions are met, the x-ray is switched on to acquire a projection image, and the gantry is then rotated to await the next synchronized event.

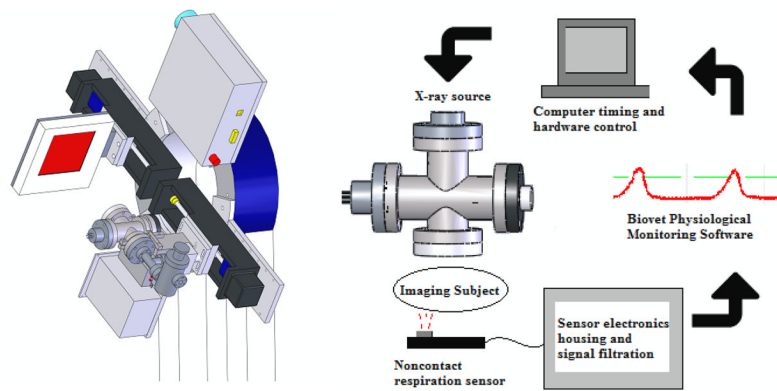


Figure 3.

The custom-built CNT cone beam micro-CT used in this study (left) consists of a compact field-emission x-ray source and flat panel detector mounted adjacent to one another on a rotating gantry. The sensor is integrated into the complete hardware of the micro-CT system as in the flowchart above (right). The sensor's output is fed into Biovet and the computer's timing program, so that appropriate physiological gating can be achieved with the x-ray source

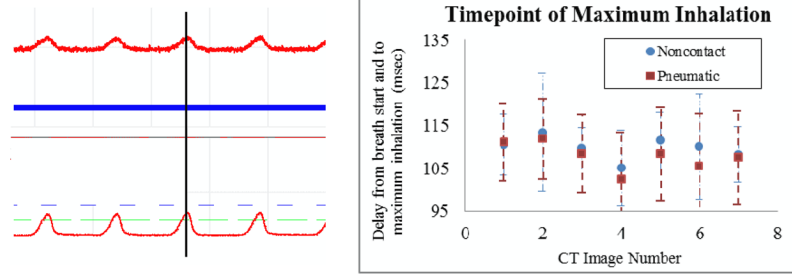


Figure 4.

Left. Simultaneously-acquired respiration traces from the standard pressure sensor (top) with x20 signal amplification and the non-contact displacement sensor (bottom) with x2 amplification are displayed in the BioVet GUI. Note the similar signal shapes and, in particular, the temporally-matching peaks corresponding to the full inhalation phase of the animal’s respiratory cycle. Additionally, the signal from the non-contact sensor is strong enough that much less signal amplification is required, resulting in a higher signal-to-electrical noise ratio when compared with the pressure sensor. **Right.** For seven CT scans, the signal traces from both respiration sensors were analysed to define the timepoint of maximum sensor output (ms) for each breath. The average over all breaths of the elapsed time between the beginning of the breath cycle to the signal peak was determined, as well as the standard deviation. The average temporal location of this peak measured for each of the two devices agreed within 5 milliseconds. Error bars for both methodologies are displayed. The large errors result from variation amongst breaths in a single scan and from signal noise, the difference in timing from the two signals is insignificant with respect to these uncertainties.

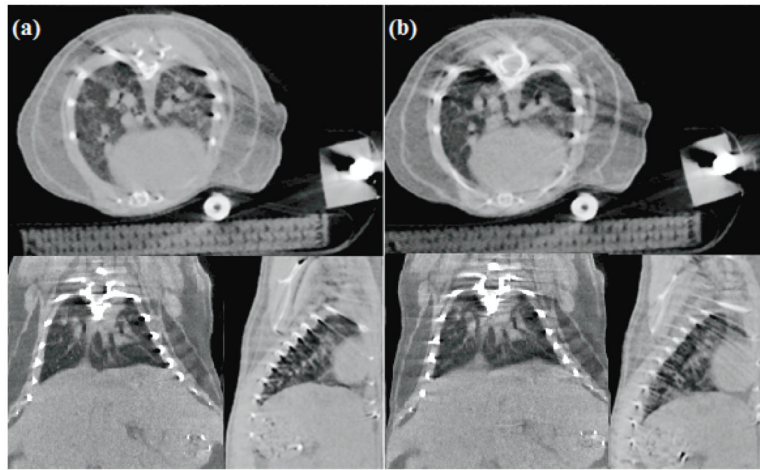
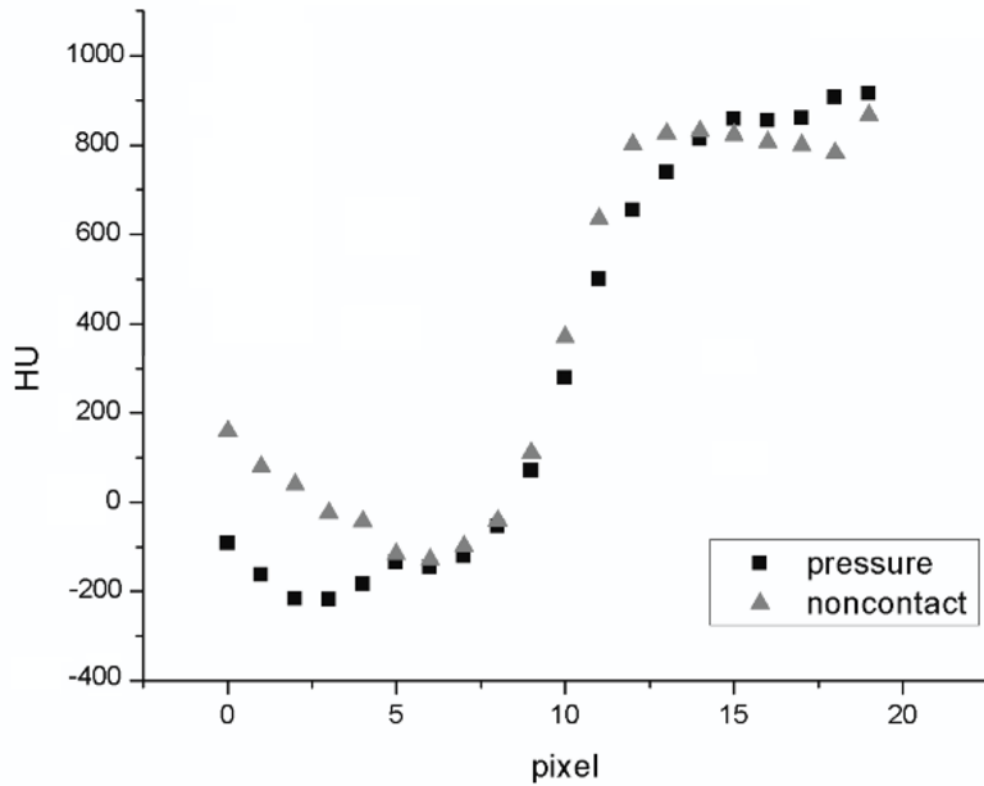


Figure 5. Transverse, coronal, and sagittal CT slices of an adult wild-type using the non-contact (a) and pressure (b) sensors to monitor and prospectively gate to respiratory motion. During the acquisition of each image, both the fiber-optic cable from the displacement sensor and the plastic tubing from the pneumatic sensor were included in the field of view so that image artifacts arising from these structures would be comparable between the two scans.

Line Plot Across Boundary of Diaphragm and Right Lung

**Figure 6.**

Line plots were measured across the lung/diaphragm boundary at four different locations in the left and right lungs (two line plots per lung) for each image acquired. The slope of the path across the boundary was measured for each gating protocol (pressure or noncontact sensor) and compared for each of the four subjects. Displayed above are a pair of right-lung/diaphragm line plots for a single subject; in this case the steeper transition in the noncontact gated image indicates reduced diaphragm motion blur as compared against the pressure sensor gated image.

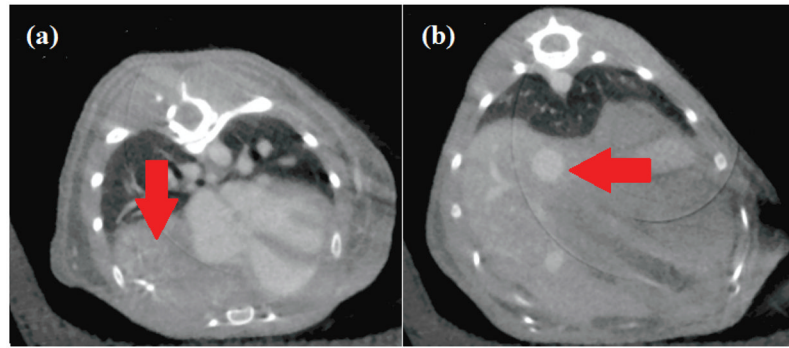


Figure 7. Respiration-gated micro-CT of the knockout hernia model. In the mid-lung axial slice (a), the liver has displaced the right lung (image left, arrow indicates duodenum where the lung would be located in a healthy animal). In what should be the mid-liver slice (b), an arrow indicates where the bowels and lower organs have moved anterior in the body and are in contact with the lower parenchyma of the lungs.

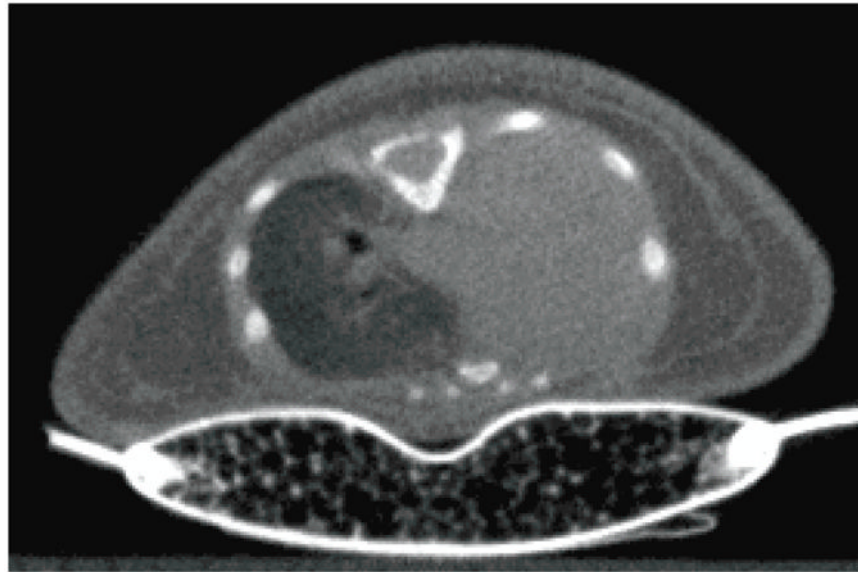


Figure 8.

A prospectively-gated CT image of a 9-day-old mouse pup using the pressure-based sensor to monitor and gate to respiration motion. The pressure required for use of this sensor results in high rates of atelectasis in the left lung (seen here as a complete pneumothorax).

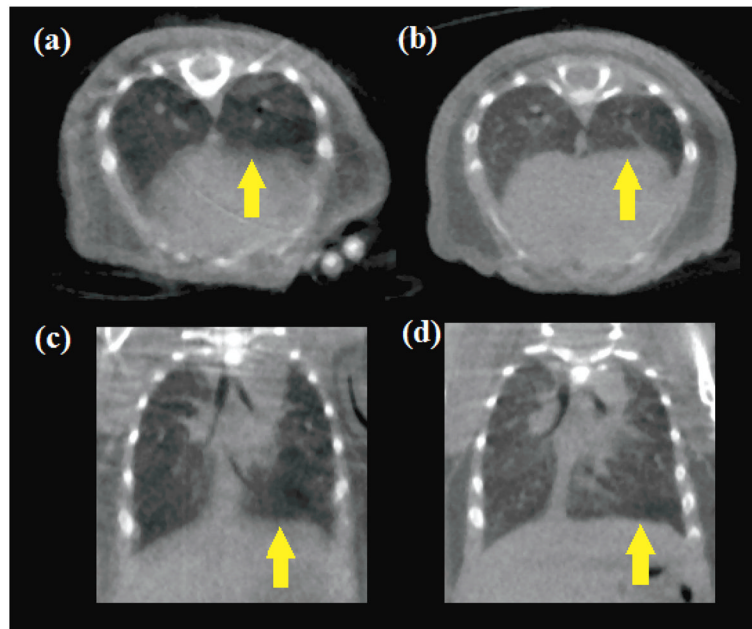


Figure 9. CT transverse and coronal slices of 11-day-old mouse pups imaged without respiration gating in (a) and (c), and using prospective respiration gating from the laser-displacement non-contact sensor in (b) and (d). Fine details of the lungs are more clearly visualized with respiration gating, as is the definition between lungs and diaphragm (indicated with arrows).

Table 1

Diaphragm slopes for control subjects with physiological gating from each respiration sensor. Two separate lines were traced from each of the left and right lungs to the diaphragm (four lines total per CT image) to obtain average slope values

	Non-contact Diaphragm Slope (HU/ pixel)	Standard Deviation	Pressure Diaphragm Slope (HU/ pixel)	Standard Deviation
M1	167	45	117	39
M2	107	49	192	95
M3	149	62	146	46
M4	142	30	106	18
All Subjects	141	48	140	61